V. Summary

Many bilevel images can be transformed into a sparse binary image by preprocessing. An easily implemented image differencing operation was presented that decorrelates the bilevel image prior to block coding. This simple differencing method combined with well-known block coding techniques extends the application areas of these techniques to a wider variety of images.

Acknowledgment

The authors thank the anonymous reviewers for carefully reading the manuscript and providing a number of constructive comments.

References

[1] G. Zeng and N. Ahmed, "A block coding technique for encoding sparse binary patterns," *IEEE Trans. Acoust., Speech, Signal Processing*, vol. 37, no. 5, pp. 778–780, May 1989.
[2] B. Y. Kavalerchik, "Generalized block coding of black and white images," *IEEE Trans. Image Processing*, vol. 1, no. 4, pp. 518–520, Oct. 1992.
[3] M. Kunt and O. Johnsen, "Block coding of graphics: A tutorial review," *Proc. IEEE*, vol. 68, no. 7, pp. 770–786, July 1980.
[4] D. Huffman, "A method for the construction of minimum-redundancy codes," *Proc. IRE*, vol. 40, pp. 1098–1101, Sept. 1952.
[5] S. W. Golomb, "Run-length encoding," *IEEE Trans. Inform. Theory*, vol. IT-12, no. 4, pp 399–401, July 1966.
[6] M. Rabbani and P. W. Jones, *Digital Image Compression Techniques*. Bellingham, WA: SPIE, 1991.
[7] M. Kunt, "Statistical models and information measurement for two-level digital facsimile," *Inform. Contr.*, vol. 33, no. 4, pp. 333–351, Apr. 1977.
[8] ——, "A statistical model for correlation functions of two-level digital facsimile," *Proc. IEEE*, vol. 63, no. 2, pp. 327–329, Feb. 1975.
[9] *Tiff Specification Revision 6.0*, Aldus Corporation, June 1992.
[10] N. S. Jayant and P. Noll, *Digital Coding of Waveforms: Principles and Applications to Speech and Video*. Englewood Cliffs, NJ: Prentice-Hall, 1984.
[11] D. Bodson, K. R. McConnel, and R. Schaphorst, *FAX: Digital Facsimile Technology Applications*, 2nd ed. Norwood, MA: Artech House, 1992.
[12] R. B. Arps and T. K. Truong, "Comparison of international standards for lossless still image compression," *Proc. IEEE*, vol. 82, no. 6, pp. 889–899, June 1994.

Multidirectional and Multiscale Edge Detection via M-Band Wavelet Transform

Turgut Aydın, Yücel Yemez, Emin Anarım, and Bülent Sankur

***Abstract*— In this correspondence, the problem of directional and multiscale edge detection is considered. Orthogonal and linear-phase M-band wavelet transform is used to decompose the image into $M \times M$ channels. These channels are then combined such that each combination, which we refer to as *decomposition filter*, results in zero-crossings at the locations of edges corresponding to different directions and resolutions, and inherently performs regularization against noise. By applying a zero-crossing detector on the outputs of the decomposition filters, edge maps of desired resolution and direction are obtained. In addition, with the application of the Teager's energy operator at the analysis stage, it is possible to obtain a reduction in unwanted zero-crossings. Final edge maps of images are obtained through simple combinations of directional edge maps.**

I. Introduction

Edge detection is defined as the problem of locating abrupt gray-level changes in a luminance image or such depth changes in a range image. If edge detection is perceived as the first step of an image understanding scheme, then simultaneous detection of edges with different orientations and at different scales becomes of interest.

The conventional approach to edge detection, that is, the detection of gray-level changes, is based on either thresholding the first derivative of the image (gradient) or locating the zero-crossings of its second derivative (Laplacian). Such operators performing these first or second derivatives have highpass characteristics, and have a tendency to emphasize noise and create spurious edge pieces. Therefore, these conventional approaches may cause difficulties in many applications. Since edge detection is an ill-posed problem, the behavior of these algorithms has been tamed via regularization scheme. An example is the Laplacian operator combined with Gaussian filters resulting in the so-called Laplacian of Gaussian (LoG) filters. An important point is that all regularized edge detectors possess bandpass filter characteristics [1]–[4]. For example, the bandwidth of a LoG filter is determined by the variance of the Gaussian smoother and by varying its bandwidth; edge maps at different scales are obtained. This approach, also called the Marr and Hildreth paradigm [4], aims to optimize the tradeoff between noise filtering and edge detection.

We conjecture that the M-band wavelet transform has the potential to perform such a multiscale multidirectional edge detection since it is, basically, a tool to view signals at different scales, and decomposes a signal by projecting it onto a family of functions generated from a single wavelet basis via its dilations and translations [5]. The image is first wavelet transformed into M^2 resolution cells by applying the M-band transform separately in the horizontal and vertical directions. Then, various combinations of these bandpass sections are taken to obtain different scales and orientations in the frequency plane. This filtering achieves the desired regularizations inherently.

Manuscript received October 14, 1994; revised November 13, 1995.
This work was supported by TÜBİTAK under contract EEEAG-139 and was partly presented in ICASSP-94, Australia. The associate editor coordinating the review of this manuscript and approving it for publication was Dr. Michael Unser.
The authors are with Boğaziçi University, Department of Electrical and Electronics Engineering, 80815, Bebek, İstanbul, Turkey (e-mail: anari@trboun.binet).
Publisher Item Identifier S 1057-7149(96)05261-X.

TABLE I
FILTER COEFFICIENTS FOR EIGHT-TAP FOUR-BAND WAVELET TRANSFORM

n	$\psi_1(n)$	$\psi_2(n)$	$\psi_3(n)$	$\psi_4(n)$
0	-0.067371764	-0.094195111	-0.094195111	-0.067371764
1	0.094195111	0.067371764	-0.067371764	-0.094195111
2	0.40580489	0.56737176	0.56737176	0.40580489
3	0.56737176	0.40580489	-0.40580489	-0.56737176
4	0.56737176	-0.40580489	-0.40580489	0.56737176
5	0.40580489	-0.56737176	0.56737176	-0.40580489
6	0.094195111	-0.067371764	-0.067371764	0.094195111
7	-0.067371764	0.094195111	-0.094195111	0.067371764

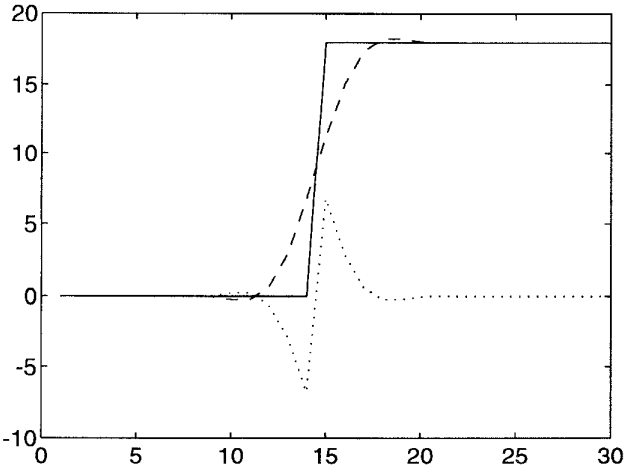

Fig. 1. Step edge (solid line), the smoothed edge (dashed line), and their difference (dotted line).

Wavelets have been used previously for multiscale edge analysis. For example, Mallat *et al.* [6] decomposed an image via regular wavelets so that the various resolution bands corresponded to the gradient of the smoothed image at different scales. The so-called singularity points are then detected as the modulus maxima.

In our approach, one novelty is that we achieve the multidirectional multiresolution edge detection filters by using the M-band wavelets. The other novelty is that we apply "unconventional" nonlinear operators, such as Teager's operator, on the decomposed images in order to enhance the "edge-to-background" ratio.

The organization of this correspondence is as follows. Section II presents the analyses of the techniques involved in the proposed edge-detection scheme, and details the algorithmic steps. In Section III, results and performance of the proposed edge detector are discussed.

II. EDGE DETECTION USING WAVELET TRANSFORM

A. One-Dimensional Analysis

To clarify our method, we first pose the problem in one dimension. The one-dimensional (1-D) analysis is also known as *residual edge detection* [7].

The difference of the smoothed versions of a step edge at two different scales results in a zero-crossing at the edge location. In general, such edge detectors can be referred to as *difference of regularized solutions* (DORS) [8]. When the wavelet filters are

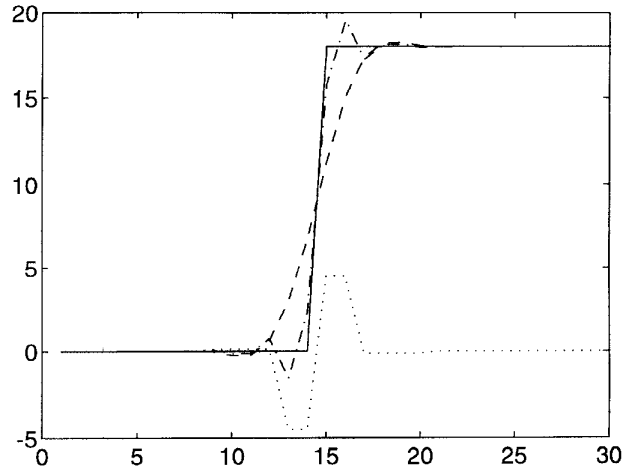

Fig. 2. Step edge (solid line), the two smoothed edges (dashed line by H_1, dashdot by $H_1 + H_2 + H_3$), and their difference (dotted line).

orthogonal and the system has a perfect reconstruction quadrature mirror filter (PR-QMF) structure with $\sum_{i=1}^{M} \Psi_i \Psi_i^* = 1$, these differences of smoothed solutions can also be obtained at the output of proper additive combinations of the filters $H_i = \Psi_i \Psi_i^*$, $i = 1, 2, \cdots M$, where Ψ_i stands for the ith band analysis filter and Ψ_i^*, the ith band synthesis filter of the wavelet transform in frequency domain. These combinations should also be chosen so that the output of each different combination views the edge information at a different resolution.

For the four-band case, one can look at the signal in the three scales which, when expressed as DORS, become (in increasing resolution order)

$$H_2 = (H_1 + H_2) - H_1 \tag{1}$$

$$H_2 + H_3 = (H_1 + H_2 + H_3) - H_1 \tag{2}$$

$$H_2 + H_3 + H_4 = (H_1 + H_2 + H_3 + H_4) - H_1. \tag{3}$$

The occurrence of a zero-crossing through (3) and (2) is illustrated in Figs. 1 and 2, respectively. The spectral behavior of the smoothing lowpass filters H_1, $H_1 + H_2$ and $H_1 + H_2 + H_3$ are displayed in Fig. 3. To be able to have consistent results and selectivity in resolution and direction, the wavelet filters are required to be flat and compact at the desired frequency band. The time-domain coefficients of the eight-tap, four-band orthogonal linear-phase wavelet filters ψ_i, designed so as to meet these requirements according to [5], are given in Table I.

Since the filters in (1) and (2) are differences of smoothing lowpass filters, regularization against noise is inherently present. On the other hand, zero-crossings will also appear at those locations where gray-level differences are not so large, corresponding to weak edges. In addition, zero-crossings will appear at nonedge locations with increasing noise levels. The use of nonlinear operators (Section II-C) is intended for filtering out those spurious edges.

B. Two-Dimensional Analysis

In extending the described methodology to the two-dimensional (2-D) case, "meaningful" combinations of the filters are selected to reflect both scale and orientation of the edges.

The M^2-channel 2-D separable wavelet transform is obtained by the tensor product of M-band 1-D wavelet filters, which are denoted by Ψ_{ij} for $i, j = 1, 2, 3, 4$ with $M = 4$. Also, the ijth resolution

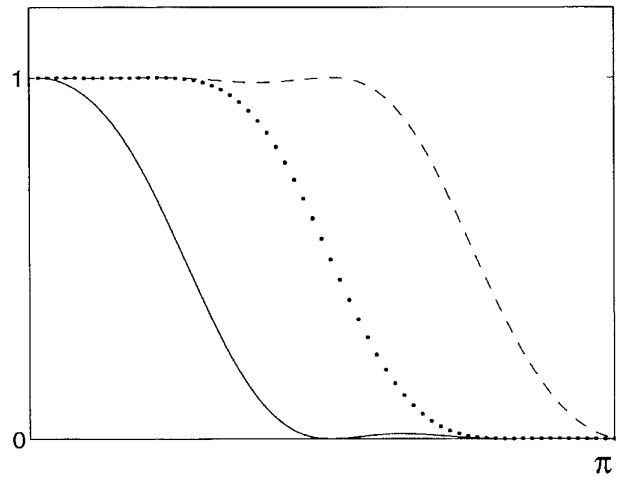

Fig. 3. The spectral behavior of the smoothing lowpass filters H_1 (solid line), $H_1 + H_2$ (dotted line), and $H_1 + H_2 + H_3$(dashed line).

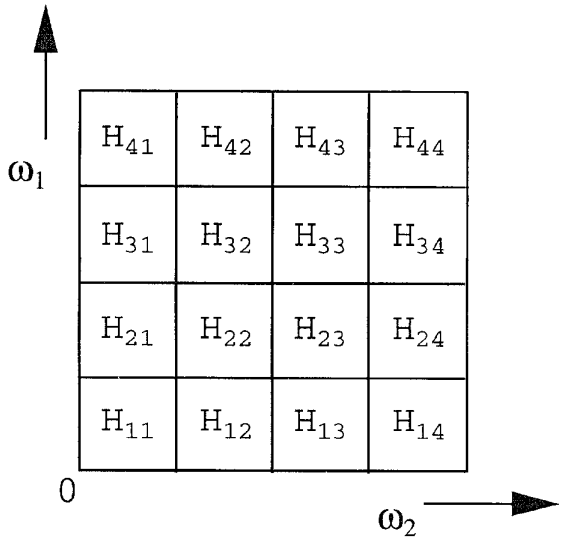

Fig. 4. Frequency bands corresponding to decomposition filters.

cell is achieved via the filter $H_{ij} = \Psi_{ij}\Psi_{ij}^*$ for $i, j = 1, 2, 3, 4$ with $M = 4$. The decomposition of the image into 16 channels is illustrated in Fig. 4. Recall that the spectral response to edges is strongest in the direction perpendicular to the edge, while it decreases as the look direction of the filter is aligned with the edge. Therefore, we can perform edge enhancement by using 2-D filters that are highpass along the edge direction and lowpass along the orthogonal direction. The frequency response of a typical edge-enhancing filter covers a sector in the 2-D spatial frequency domain as shown in Fig. 5 [3]. The meaningful combinations of the wavelet decomposition filters are based on this frequency sector concept and correspond to the summations $\sum_R H_{ij}$, where R denotes the frequency sector of a certain direction and resolution. We should note that these summations are approximations to frequency sectors and actually contain tiles of frequency.

Since our system is orthogonal, and has PR-QMF structure, that is, $\sum_{i=1}^{M}\sum_{j=1}^{M}\Psi_{ij}\Psi_{ij}^* = 1$, the summation $\sum_R \Psi_{ij}\Psi_{ij}^*$ makes sense and results in 2-D filters of desirable form, which treats all the frequencies in a resolution cell as equally as possible.

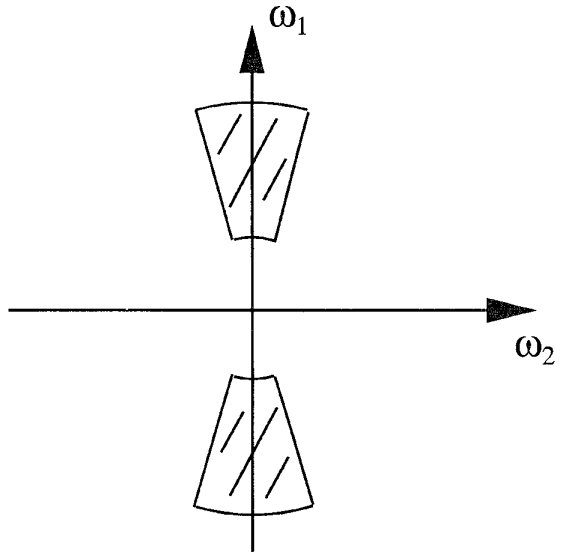

Fig. 5. Frequency sector representation for filtering in horizontal direction.

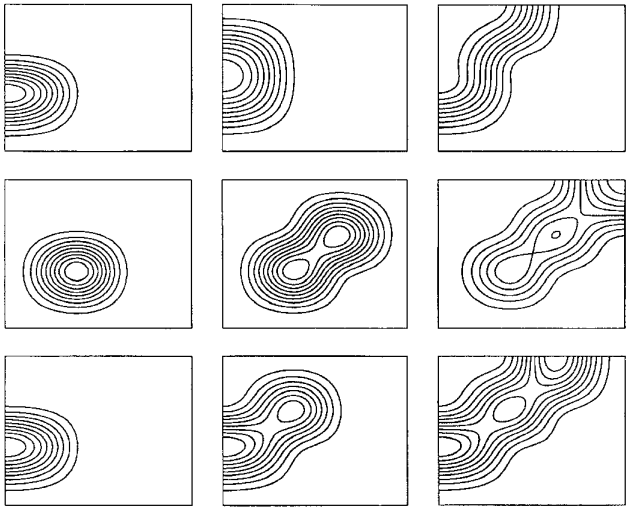

Fig. 6. In increasing resolution. Top row, vertical; middle row, diagonal; bottom row, vertical-diagonal decomposition filters in frequency plane. (See Fig. 4 for comparison.)

The number of channels and, therefore, the number of possible filter combinations depend on the number of bands, which in turn determines the size of the selectivity in direction and scale. Some of the decomposition filters $\sum_R H_{ij}$ are displayed in Fig. 6 and are formed as follows for different directions in increasing resolution (see also Fig. 4).

- Horizontal direction:

$$F_{H1} = H_{12}$$
$$F_{H2} = H_{12} + H_{13}$$
$$F_{H3} = H_{12} + H_{13} + H_{14} + H_{24}$$

- Vertical direction:

$$F_{V1} = H_{21}$$
$$F_{V2} = H_{21} + H_{31}$$
$$F_{V3} = H_{21} + H_{31} + H_{41} + H_{42}$$

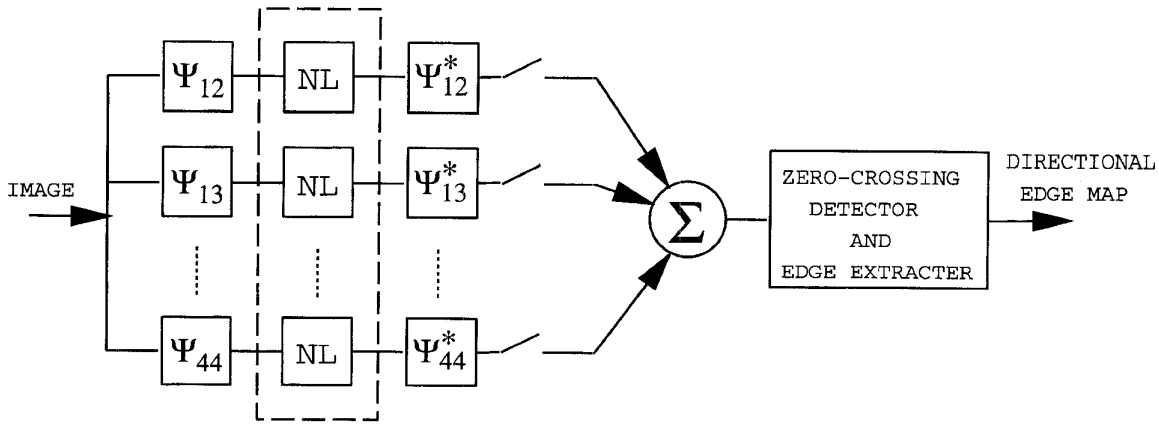

Fig. 7. Block diagram of M-band wavelet-based edge detection method.

- Diagonal direction:

$$F_{D1} = H_{22}$$
$$F_{D2} = H_{22} + H_{33}$$
$$F_{D3} = H_{22} + H_{33} + H_{44}$$

- Horizontal-diagonal direction:

$$F_{HD1} = H_{12}$$
$$F_{HD2} = H_{12} + H_{23}$$
$$F_{HD3} = H_{12} + H_{23} + H_{34}.$$

Similarly, there are also vertical-diagonal direction filters that are symmetrical counterparts of those for the horizontal-diagonal direction.

All of the above 2-D filters are bandpass filters and, therefore, recalling our 1-D analysis, each filtering operation results in zero-crossings at the location of step edges, matching the direction and resolution of that filter. Once the input image has been decomposed into its components in $M \times M$ different channels, a zero-crossing detector is applied on these components, and the initial edge maps at different resolutions and directions are obtained. By-products of this operation are false zero-crossings resulting from the Gibbs phenomenon (See Figs. 1 and 2). However, these false zero-crossings are relatively small in magnitude and therefore can be eliminated by a simple thresholding mechanism before labeling a zero-crossing as an edge pixel. In order to further eliminate resulting Gibbs phenomenon, the local variance of the original image has also been incorporated in the decision stage. A final edge map is also obtained by combining edge maps of different directions and resolutions, or by simply taking the superpositions.

C. Nonlinear Operators

The multiresolution decomposition also avails us of the possibility to apply nonlinear operations in the subbands before the final synthesis for the purposes of enhancement. These operations may distort the image at the advantage of edges, but perfect reconstruction is not eventually required anyway. However, phase linearity is essential in obtaining correctly located edges. It is also important to note that the proposed system is orthogonal and preserves the energy since the wavelet transform used is unitary. Therefore, the effect of nonlinear operations on performance is kept as small as possible. Teager's energy operator is such a nonlinear operator that can be used at this step to improve the performance of edge detection. It is defined in one dimension [9] as

$$\mathcal{T}[f(t)] = (\frac{df(t)}{dt})^2 - f(t)\frac{d^2 f(t)}{dt^2} \tag{4}$$

while in discrete domain, the operator becomes

$$\mathcal{T}[f(n)] = f^2(n) - f(n+1)f(n-1). \tag{5}$$

Rather than searching for a 2-D version of this energy operator, the above 1-D energy operator is utilized at the output of each of the 2-D analysis stage. Thus, after the application of Teager's energy operator on the outputs of the filters Ψ_{ij}, pixel values are thresholded so that only the highly "energetic" edge locations are fed into the interpolating filters. The resulting image is not the reconstruction of the original anymore; false zero-crossings are mostly eliminated and edge-detection performance is improved.

D. Algorithm

The edge-detection algorithm based on the M-band wavelet decomposition and Teager enhancement is illustrated in the block diagram (Fig. 7).

This algorithm consists of the following steps.

- The input image is first decomposed into $M \times M$ channels by the wavelet analysis stage without downsampling. Unlike other edge detection algorithms based on wavelet transforms, edge information is not extracted at this stage. These outputs, are subjected to Teager's energy operator followed by background thresholding. In this way, details containing less energy are supressed and edgelike evidences are corroborated.
- These nonlinearly treated individual bands are then followed by the synthesis stage (inverse wavelet transform). Linear combinations of these channels are selected to constitute the desired edge-detection filters with various scales and directions.
- The outputs of the edge-detection filters are the zero-crossing magnitude images. Zero-crossing maps are obtained by thresholding these images so as to eliminate the unnecessary zero-crossing pixels while the threshold is adjusted to the statistics of the zero-crossing magnitudes. Further refinement of these zero-crossing maps by masking with respect to local variance values of the original image results in the edge maps of different directions and resolutions. The combination of a horizontal and a vertical edge map with various directions or scales yields a complete edge map of the image. The combinations may be based on various directions or scales.

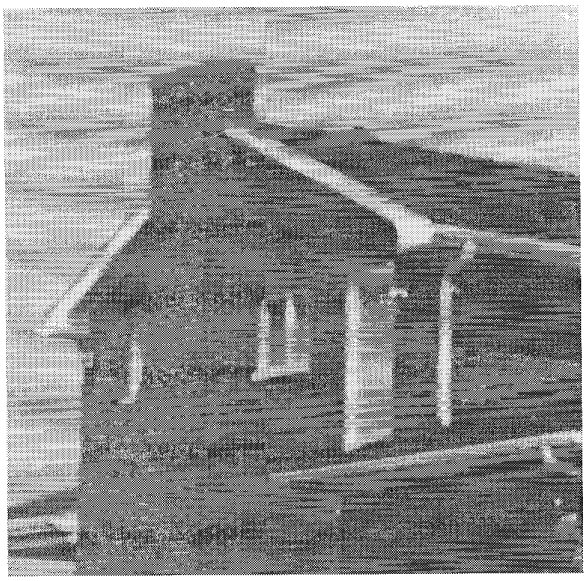

Fig. 8. Original house image.

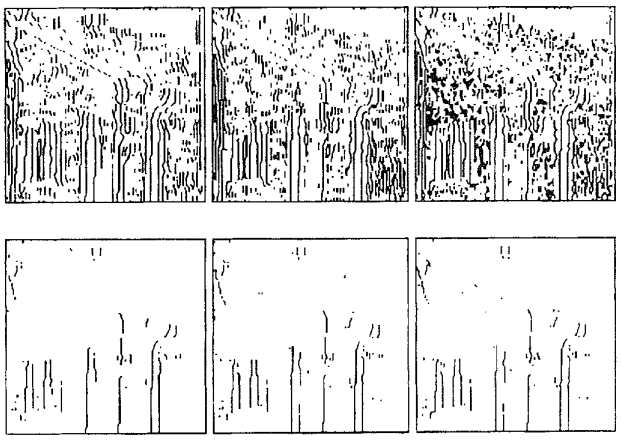

Fig. 9. In increasing resolution from top left to bottom right. Top row: zero-crossings corresponding to vertical edge candidates. Bottom row: vertical edges.

III. Experimental Results

Our test image is a 128×128 window of the House image shown in Fig. 8. In Figs. 9–11, we display the zero-crossings and the edge maps corresponding to different resolutions and directions. These edge maps are obtained with a 16-channel decomposition using four-band linear phase orthogonal filter banks as in [5], and the filter combinations are chosen as in Section II-B In these figures, we observe that as the resolution is reduced, some of the details of the original image, e.g., the shadow of the roof, are lost as expected. The effects of the edge enhancement operation via Teager's energy operator followed by thresholding are illustrated in Figs. 12–14. In these maps, the diagonal Teager's operator is defined as

$$\mathcal{T}[f(n,m)] = \max\{f^2(n,m) - f(n-1,m-1)f(n+1,m+1) \quad (6)$$
$$f^2(n,m) - f(n-1,m+1)f(n+1,m-1)\}$$

Similarly, it is also possible to define Teager's operator for horizontal-diagonal and vertical-diagonal directions if a window size larger than 3 × 3 is chosen.

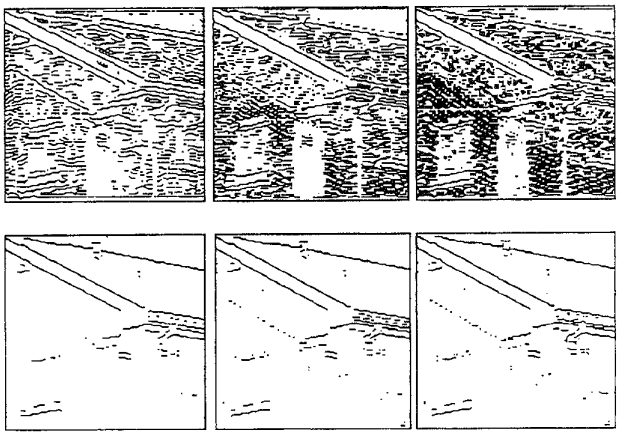

Fig. 10. In increasing resolution from top left to bottom right. Top row: zero-crossings corresponding to horizontal edge candidates. Bottom row: horizontal edges.

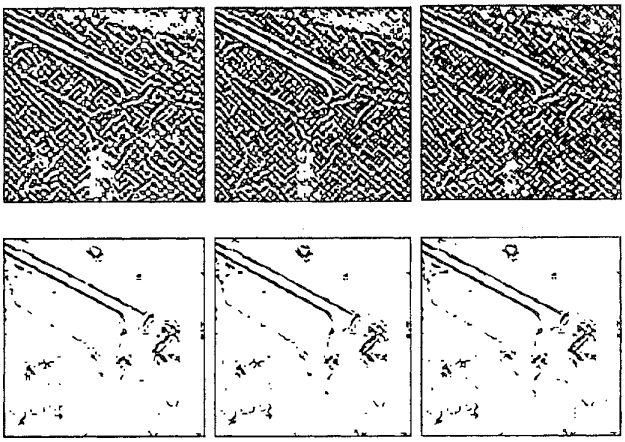

Fig. 11. In increasing resolution from top left to bottom right. Top row: zero-crossings corresponding to diagonal edge candidates. Bottom row: diagonal edges.

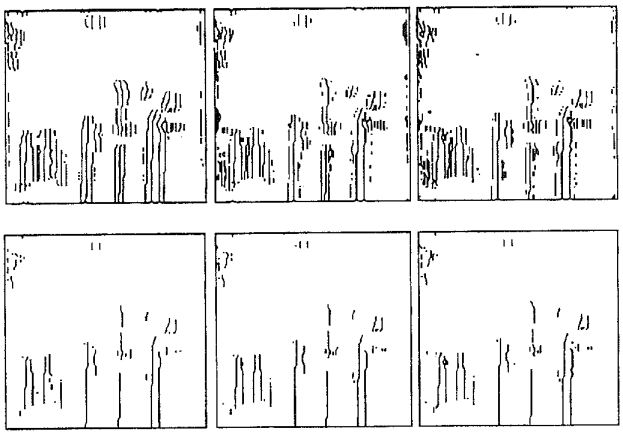

Fig. 12. Incorporating Teager's operator (in increasing resolution). Top row: zero-crossings corresponding to vertical edge candidates. Bottom row: vertical edges.

Notice that the resulting edge maps contain less spurious details, especially in the horizontal and diagonal cases. Finally, the combined

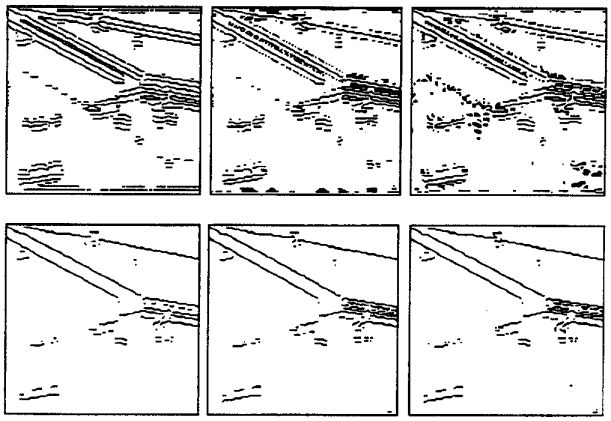

Fig. 13. Incorporating Teager's operator (in increasing resolution). Top row: zero-crossings corresponding to horizontal edge candidates. Bottom row: horizontal edges.

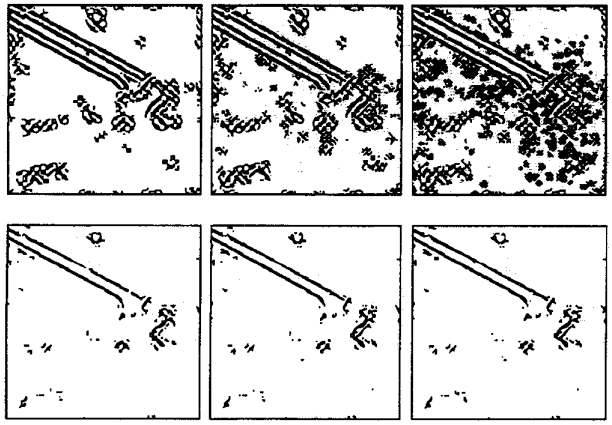

Fig. 14. Incorporating Teager's operator (in increasing resolution). Top row: zero-crossings corresponding to diagonal edge candidates. Bottom row: diagonal edges.

edge maps with and without Teager's operator, which are obtained by the union of the vertical and horizontal edge maps in low and high resolutions, are shown in Fig. 15. It is interesting to note that the edge locations that are supplied from various channels are coherent, and the edges are correctly placed.

It is desirable to maintain quantitative evaluations on edge-detection performance for the sake of comparison. Nevertheless, the subjective nature of the definition of an approach like edge detection means that it is not possible or realistic to come up with a unique measure of quality. As a result, more than one approach to evaluate performance of an edge detector exist, and the two most commonly accepted measures for edge detection are based on the following criteria:

- good localization; i.e., accuracy of estimated edge location;
- good detection; i.e., unique response to edge points and no response to nonedge points.

A measure of localization performance [10]–[12] is given by

$$P_l = \frac{1}{\max(n_d, n_o)} \sum_{i=1}^{n_d} \frac{1}{1 + \alpha d_i^2}$$

where n_d is the number of detected edge points, n_o is the number of original edge points, α is a calibration constant, d_i is the Euclidian distance between an edge pixel (detected edge point) denoted by

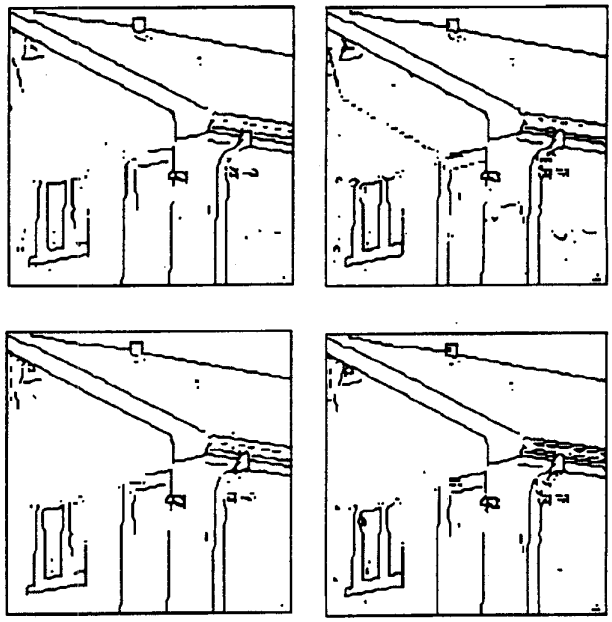

Fig. 15. In increasing resolution: Top row, union of vertical and horizontal edge maps; bottom row, union of vertical and horizontal edge maps, obtained by incorporating Teager's operator.

index i in the distorted image and the corresponding one (original edge point) in the reference edge map.

The detection performance can be measured as follows:

$$P_e = \frac{n_e}{n_o}$$

where n_o is the number of original edge points and n_e is the number of erroneous edge points.

These measures, unfortunately, cannot quote the quality of a given edge map as it is, but rather make comparisons to a reference edge map. Only when synthetic test images of step edge shapes (like the popular Checkerboard image) are used is it possible to evaluate the performance of an edge detector directly, since edge locations are well defined for these images.

The performance of the edge-detection method for increasing additive Gaussian white noise levels has been tested, and the results are displayed in Figs. 16 and 17. The reference edge map in these experiments has been obtained by the application of edge detection onto the noiseless image. For the case with Teager's operator, the reference edge has also been obtained with Teager's operator present in edge-detection procedure. Since incorporation of Teager's operator changes the nature of the edge detector and numerical performance depends on the reference edge map, a quantitative comparison of the two schemes is not meaningful. Instead, the trends shown by the two curves should be compared.

The results indicated by the performance curves may be grouped as follows.

- Both edge-detection schemes show immune behavior with respect to noise: The curves reflect smooth deterioration rather than a sharp drop under increasing noise levels.
- Incorporation of Teager's operator increases immunity to noise: The declining performance trend is decelerated when Teager's operator is present. In other words, the detected edges under the presence of noise is more similar to the detected edges under noiseless conditions when Teager's operator is utilized.

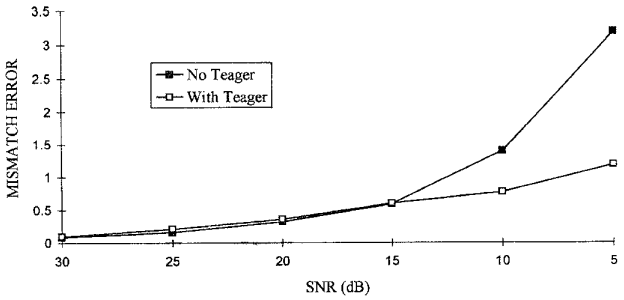

Fig. 16. Detection performance of the edge-detection scheme against white Gaussian noise.

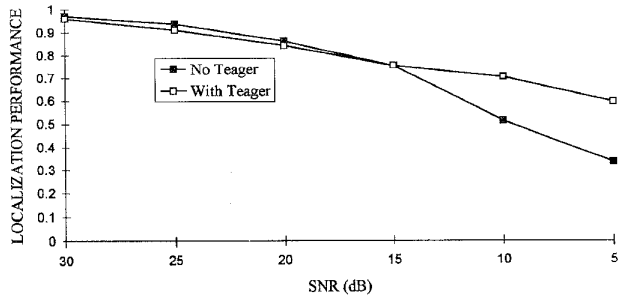

Fig. 17. Localization performance of the edge-detection scheme against white Gaussian noise.

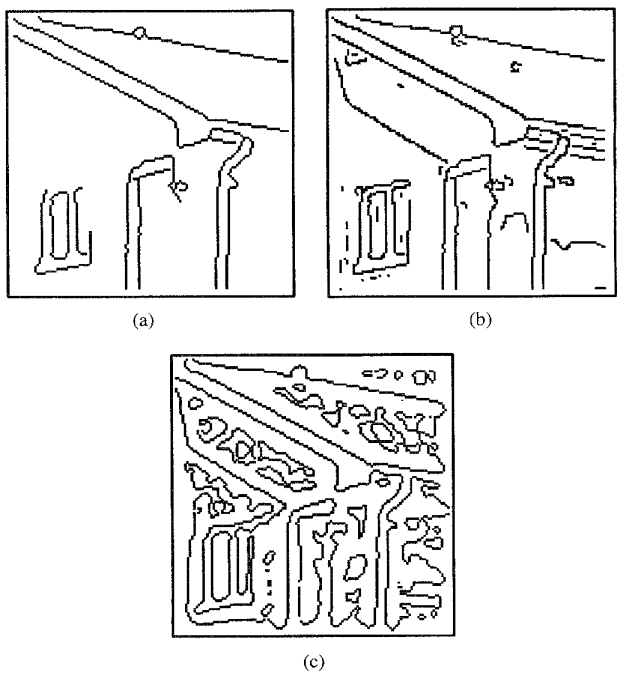

Fig. 18. Edge maps obtained by (a) Canny's edge detector; (b) Canny's edge detector with relaxed connectivity constraint; (c) Marr–Hildreth's edge detector.

Edge detection results of Canny's edge detector and Marr–Hildreth edge detector are also illustrated in Fig. 18 for subjective evaluation. The wavelet-based scheme should be regarded as the filtering stage of a more intelligent edge-detection scheme such as Canny's edge detector [1], by which the zero-crossings leading to edge pixels are extracted and classified. Therefore, the performance of our scheme can certainly be improved by employing some decision-based rules on the edge maps of different directions and resolutions, and/or by imposing connectivity constraints for being an edge pixel, as in Canny's edge detector. The Marr–Hildreth [4] edge detector [Fig. 18(c): $\sigma = 1.2$, mask size = 17] without extra control finds most of the edges, but also results in many unwanted details. The Canny edge detector [Fig. 18(a): $\sigma = 1$, mask size = 9], on the other hand, exhibits a very "clean" edge map, but loses some important details. When the connectivity constraints are relaxed, the Canny edge detector performance increases in terms of preserving details, but noise edges dramatically increase [Fig. 18(b)].

Under subjective evaluation, the compared edge-detection schemes would each find support depending on the subjective definition or quality criteria put forward by the evaluator. Quantitative comparison of different schemes with each other would, on the other hand, be meaningful only if there had been a reference edge map to compare against; however, it is not possible to define a reference edge map for real scenery without ambiguity. Furthermore, all these edge detectors function differently depending on the parameters that control each detector's peculiarities. For example, control of "scale" involves the adjustment of variance of the Gaussian in the Marr–Hildreth detector, while Canny suggests use of multiple-width edge masks and adjustable decision thresholds for connectivity control.

IV. Conclusion

In this correspondence, a new method for edge detection by using M-band wavelet transform and an energy operator has been presented, and its performance has been analyzed.

Following is a summary of the advantages of our method.

- The method is multiscale and multidirectional in the sense that it decomposes the edge information into various scales and directions.
- Since the filter bank is linear phase and orthogonal, the performance is not degraded through the use of nonlinear operations, and it becomes possible to incorporate Teager's operator between the analysis and synthesis stages to enhance the edges of different scale and resolution independently.
- The filters can be designed so as to be compact and flat in a frequency band and, therefore, the method is selective in frequency and direction. In addition, the decomposition filters are of desirable form and treat all the frequencies as equally as possible.
- Edge pixels are always correctly placed.
- Regularization against noise is inherently present.

Acknowledgment

The authors wish to acknowledge TÜBİTAK for their support during this work. The authors are also grateful to M. Unser on the Editorial Board for his thoughtful guidance in revising the manuscript, and the referees for their constructive review and valuable comments.

References

[1] J. Canny, "A computational approach to edge detection," *IEEE Trans. Pattern Anal. Machine Intell.*, vol. PAMI-8, no. 6, pp. 679–697, Nov. 1986.

[2] V. Torre and T. Poggio, "On edge detection," *IEEE Trans. Pattern Anal. Machine Intell.*, vol. PAMI-8, no. 4, pp. 147–163, 1986.

[3] A. Ikonomopoulos and M. Kunt, "Image coding via directional filtering," *Signal Processing*, vol. 8, no. 2, pp. 179–202, Apr. 1985.

[4] D. Marr and E. C. Hildreth, in *Proc. Roy. Soc. London, Series B, Theory of Edge Detection*, 1980, vol. 207, pp 187–217.

[5] O. Alkın and H. Çağlar, "Design of efficient M-band coders with linear-phase and perfect-reconstruction properties," *IEEE Trans. Signal Processing*, vol. 43, no. 7, pp. 1579–1590, July 1995.
[6] S. Mallat and W. L. Hwang, "Singularity detection and processing with wavelets," *Trans. Inform. Theory*, vol. 38, no. 2, pp. 617–643, Mar. 1992.
[7] M. Chen, D. Lee, and T. Pavlidis, "Residual analysis for feature detection," *IEEE Trans. Pattern Anal. Machine Intell.*, vol. 13, no. 1, pp. 30–40, 1991.
[8] M. Gökmen and C. Li, "Multiscale edge detection using first order R-filter," in *Proc. IEEE Conf. Pattern Recog.*, The Netherlands, 1992. pp. 307–310.
[9] J. F. Kaiser, "On a simple algorithm to calculate the energy of a signal," in *Proc. IEEE ICASSP-90*, Albuquerque, NM.
[10] A. K. Jain, *Fundamentals of Digital Image Processing.* Englewood Cliffs, NJ: Prentice-Hall, 1989.
[11] L. Kitchen and A. Rosenfeld, "Edge evaluation using local edge coherence," *IEEE Trans. Syst., Man, Cybern,* vol. SMC-11, no. 9, pp. 597-605, 1981.
[12] W. Lunscher and M. Bodoes, "Optimal edge detector evaluation," *IEEE Trans. Syst., Man, Cybern.,* vol. SMC-16, no. 2, pp. 304-312, 1986.

Steerable Wedge Filters for Local Orientation Analysis

Eero P. Simoncelli and Hany Farid

***Abstract*—Steerable filters have been used to analyze local orientation patterns in imagery. Such filters are typically based on directional derivatives, whose symmetry produces orientation responses that are periodic with period π, independent of image structure. We present a more general set of steerable filters that alleviate this problem.**

I. Introduction

Oriented linear filters are used in many vision and image processing tasks such as edge detection, segmentation, texture analysis, and motion analysis. Their basic behavior with regard to representation of orientation may be examined by computing an "orientation map:" the squared filter response as a function of filter orientation (e.g., [2]–[4], [8]). Such filters are almost always either symmetric or antisymmetric. The symmetry (or antisymmetry) of the filters imposes a periodicity of period π on the orientation map, regardless of the underlying image structure. For example, an orientation map computed at the end of a line segment will produce a *bimodal* response. Such an ambiguity is undesirable for many applications. For this reason, some authors have recently begun to explore the use of asymmetric filters for orientation analysis [6], [7], [9].

A secondary theme in this sort of orientation analysis is that of rotation-invariance [1], [2], [4], [5], [7]. Along these lines, Freeman and Adelson developed the concept of *steerable filters*, in which an oriented filter is synthesized *exactly* from a linear combination of a fixed set of basis filters. They constructed such bases using directional derivatives of Gaussians, and used these filters to compute local orientation maps. But directional derivatives of Gaussians are either symmetric or antisymmetric, and thus they suffer from the periodicity problem mentioned above.

In this article, we describe a new class of filters for local orientation and junction analysis. These filters are both asymmetric and steerable, and are designed to produce an optimally localized oriented energy map. A preliminary report of this work has been presented in [10].

Manuscript received January 13, 1995; revised September 21, 1995. This work was supported by ARPA Grant N00014-92-J-1647, ARO Grant DAAL03-89-C-0031PRI, and NSF Grant CISE/CDA-88-22719. The associate editor coordinating the review of this manuscript and approving it for publication was Prof. Moncef Gabbouj.

The authors are with GRASP Laboratory, Dept. of Computer and Information Science, University of Pennsylvania, Philadelphia, PA 19104 USA (e-mail: eero@central.cis.upenn.edu).

Publisher Item Identifier S 1057-7149(96)05255-4.

II. Steerability and Orientation Maps

This section gives a brief overview of the principle of steerability, and describes its use in computing orientation maps. The simplest example of a steerable filter is the partial derivative of a two-dimensional (2-D) Gaussian. In polar coordinates, the horizontal and vertical derivatives are written

$$G_1^{(0)}(r,\theta) = \cos(\theta)(-re^{-r^2/2})$$
$$G_1^{(\pi/2)}(r,\theta) = \sin(\theta)(-re^{-r^2/2})$$

where the subscript indicates the derivative order and the parenthesized superscript indicates the derivative direction. It is well known (and easy to verify, using basic trigonometric identities) that $G_1(r,\theta)$ can be synthesized at an arbitrary orientation, ϕ, using the following equation:

$$G_1^{(\phi)}(r,\theta) = \cos(\phi)G_1^{(0)}(r,\theta) + \sin(\phi)G_1^{(\pi/2)}(r,\theta). \quad (1)$$

This equation embodies the steerability of these functions: The directional derivative G_1 can be generated at an arbitrary orientation ϕ via a linear combination of the rotated *basis filters*, $G_1^{(0)}$ and $G_1^{(\pi/2)}$. The coefficients $\cos(\phi)$ and $\sin(\phi)$ are referred to as the *interpolation functions*. Since convolution is a linear operation, the result of convolving with an arbitrarily oriented filter may be computed via a linear combination of the results of convolving with the basis filters.

Steerability is not limited to first derivative functions. The general steerability condition, for polar-separable functions, is written as

$$f^{(\alpha)}(r,\phi) = h(\phi-\alpha)g(r) = \sum_{n=1}^{\hat{N}} k_n(\alpha)h(\phi-\alpha_n)g(r) \quad (2)$$

where $h(\cdot)$ is the angular portion of the steerable filter, $g(\cdot)$ is the radial portion, $k_n(\cdot)$ are interpolation functions, and α_n are a fixed set of $\hat{N}$ orientations. Freeman and Adelson [2] showed that this equation is satisfied by all functions with angular components that are bandlimited to contain no more than $\hat{N}/2$ harmonic terms. They presented examples of steerable filter sets consisting of higher order directional derivatives of a Gaussian, along with steerable approximations to their Hilbert transforms.

Results of applying a steerable fourth-order directional derivative of a Gaussian and an approximation to its Hilbert transform[1] to several synthetic images are shown in Fig. 1. Orientation maps are computed as the sum of squared responses of these filters. The maps of the vertical line and cross are as expected. However, the filters respond bimodally to the half-line at $\phi = \pi/2$ and $\phi = 3\pi/2$ (instead of exhibiting a single peak at $\phi = \pi/2$). The response to the corner is

[1]These filters are used in [2] and are notated as G_4/H_4.